

Efficient Planar Pose Estimation via UWB Measurements

Haodong Jiang¹, Wentao Wang², Yuan Shen³, Xinghan Li², Xiaoqiang Ren⁴, Biqiang Mu⁵, and Junfeng Wu¹

Abstract—State estimation is an essential part of autonomous systems. Integrating the Ultra-Wideband (UWB) technique has been shown to correct the long-term estimation drift and bypass the complexity of loop closure detection. However, few works on robotics treat UWB as a stand-alone state estimation solution. The primary purpose of this work is to investigate planar pose estimation using only UWB range measurements and study the estimator’s statistical efficiency. We prove the excellent property of a two-step scheme, which says that we can refine a consistent estimator to be asymptotically efficient by one step of Gauss-Newton iteration. Grounded on this result, we design the GN-ULS estimator and evaluate it through simulations and collected datasets. GN-ULS attains millimeter and sub-degree level accuracy on our static datasets and attains centimeter and degree level accuracy on our dynamic datasets, presenting the possibility of using only UWB for real-time state estimation.

I. INTRODUCTION

A. Background

State estimation is a fundamental prerequisite for an intelligent mobile robot to realize tasks such as obstacle avoidance and path planning. In recent years, significant efforts have been devoted to achieving high-performance and real-time state estimation using onboard sensors such as IMU, cameras, and lidars. However, these methods confront issues such as long-term drift [1] and low robustness in geometrically degenerated environments [2]. To overcome the challenges mentioned above, we can integrate external information such as GPS in state estimation [3].

Ultra-Wideband (UWB) is a radio technology that can provide range measurements with centimeter to decimetre level accuracy [4]. Many recent works [5]–[8] combine UWB range measurements to realize drift-free state estimation in GPS-denied environments, and the results demonstrate that integrating UWB can eliminate the long-term drift and circumvent the complexity of loop closure detection. Traditionally, UWB is used as a localization technique [9]–[12]. Few works on robotics investigate using UWB independently for pose estimation. Earlier studies either incorporate UWB range measurements as observations in the filtering

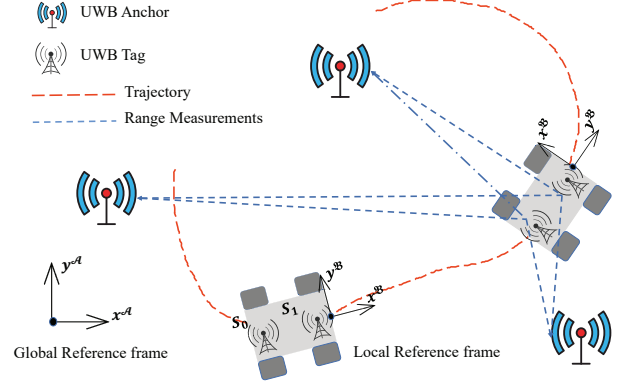


Fig. 1: Planar Pose Estimation via UWB Measurements

process [5] or as least squares factors in the optimization process [6]–[8]. We consider estimating a robot’s pose via only UWB range measurements and recognize it as the **Rigid Body Localization (RBL)** problem in the signal processing community. Through literature review, we find that the statistical efficiency of estimators has not been well studied in previous works, and the estimators’ computational complexity requires further reduction to realize real-time pose estimation.

This work investigates pose estimation using only UWB range measurements and studies the estimator’s statistical efficiency. We focus on the planar case as shown in Fig. 1, which has many critical applications such as search and rescue robots [13] and indoor service mobile robots [14]. We adopt a two-step scheme and develop a closed-form estimator, which is asymptotically efficient under mild conditions related to anchor geometry. We also conduct simulations and experiments to compare with previous methods.

B. Related Work About Planar Rigid Body Localization

The maximum likelihood (ML) formulation of RBL under i.i.d Gaussian noise assumption is a constrained weighted least squares (LS) problem (2). However, the ML estimate is difficult to obtain due to the nonconvexity and nonlinearity of (2). A common practice is to apply the least squares methodology to the squared range measurements and formulate the squared least squares (SLS) problem (6).

As far as we know, the work [15] is the first to formulate the RBL problem. The work [15] proposes to modify the SLS problem by projecting the squared measurements onto the null space of unit vectors. This operation eliminates the quadratic term and makes the problem linear, and the idea is followed by the work [16] and our work. We term the resulting formulation (7) projected squared least squares (PSLS). Based on PSLS, the work [15] solves a weighted orthogonal

¹: School of Data Science, the Chinese University of HongKong, Shenzhen, P. R. China, haodongjiang@link.cuhk.edu.cn, junfengwu@cuhk.edu.cn. ²: College of Control Science and Engineering and the State Key Laboratory of Industrial Control Technology, Zhejiang University, Hangzhou, P. R. China, {wtt1999, 11832014}@zju.edu.cn. ³: School of Electronic and Optical Engineering, Nanjing University of Science and Technology, Nanjing, P. R. China, syuan@njjust.edu.cn. ⁴: School of Mechatronic Engineering and Automation, Shanghai University, Shanghai, P. R. China xqren@shu.edu.cn. ⁵: Key Laboratory of Systems and Control, Institute of Systems Science, Academy of Mathematics and Systems Science, Chinese Academy of Sciences, Beijing, P. R. China, bqmu@amss.ac.cn

Procrustes problem by Gauss-Newton algorithms and obtains the initial value from simpler problems with closed-form solutions. The work [15] also derives the unitarily constrained Cramer-Rao lower bound (CRLB). The work [16] harnesses the structure of the rotation matrix and formulates a generalized trust region subproblem (GTRS), and the solution is refined on the linearized **SLS** problem. The work [17] uses semidefinite relaxation and formulate **SLS** as a semidefinite program (SDP). The solution is refined by one step of Gauss-Newton iteration on the **ML** problem.

To sum up, the **ML** estimate for the planar RBL problem is difficult to obtain. Previous works turn to the **SLS** problem and use different techniques to make the problem linear. However, earlier studies do not rigorously evaluate the statistical efficiency of the proposed estimators. It is only shown by simulations that the proposed estimators can achieve the CRLB over a small noise region.

C. Contributions

Although the **ML** estimate is hard to attain, we manage to design an estimator as efficient as the **ML** estimator under large samples. Noting that the sampling rate of practical UWB systems can reach up to 2.3kHz [18], our work can play a valuable role in applications. For example, the estimator can be an efficient pre-solver or initializer in a sensor-fusion scheme. The proposed estimator can also be used in decentralized multi-robot relative pose estimation.

We summarize our contributions as follows:

- (i) We design a closed-form planar pose estimator using only UWB range measurements, which has $O(n)$ computational complexity and can converge to the **ML** estimator as the measurement number n increases.
- (ii) We propose mild conditions related to anchor geometry, under which the **ML** estimator, therefore our method, can converge to the true pose with minimum variance.
- (iii) We conduct experiments in an indoor environment and elaborate on the data preprocessing procedure. To the best of our knowledge, this is the first UWB dataset suitable for the RBL problem. The dataset and code are available on our website¹.

We organize the paper as follows. Section II gives formulations of the planar RBL problem. Section III develops the **GN-ULS** estimator in two steps. Section IV gives conditions under which the **ML** estimator, therefore the **GN-ULS** estimator, is asymptotically efficient. Section V investigates different estimators' asymptotic properties via various simulations. Section V introduces data collection and discusses experiments on static and dynamic datasets. Section VII concludes the paper and discusses future works.

Notations: All vectors are column vectors and denoted by bold, lower case letters; matrices are denoted by bold, upper case letters; reference frames are denoted with $\mathcal{A}, \mathcal{B}, \mathcal{C}$. $\text{vec}(\mathbf{A})$ is a column vector by stacking the columns of \mathbf{A} . $\text{Null}(\mathbf{A})$ is the null space of \mathbf{A} . We use $\mathbf{I}, \mathbf{1}, \mathbf{0}$ to denote

identity matrices, unit vectors or matrices, and zero vectors or matrices. The symbol \odot represents the Hadamard product and \otimes the Kronecker product. For a list of vectors, we use the tuple notation $(\mathbf{v}_1, \mathbf{v}_2, \dots, \mathbf{v}_n)$ for $[\mathbf{v}_1^\top, \mathbf{v}_2^\top, \dots, \mathbf{v}_n^\top]^\top$. We use the notation \mathbf{a}° for the true value of an unknown variable \mathbf{a} . We use the notation $O_p(\mathbf{1})$ for vectors or matrices whose entries are $O_p(1)$; similarly, we use the notation $o_p(\mathbf{1})$.

II. PLANAR RIGID BODY LOCALIZATION

A. Range Measurement Model

Let \mathcal{A} be the global frame and $\mathbf{a}_m^\mathcal{A} \in \mathbb{R}^2, m \in \{1, \dots, M\}$ be the coordinates of M anchors in \mathcal{A} . Let \mathcal{B} be the local frame of the rigid body. The rigid body is fixed with N tags whose coordinates in \mathcal{B} are denoted as $\mathbf{s}_i^\mathcal{B} \in \mathbb{R}^2, i \in \{1, \dots, N\}$. The pose of \mathcal{B} with respect to \mathcal{A} can be represented by a rotation matrix $\mathbf{R}^\circ \in \text{SO}(2)$ and a position vector $\mathbf{t}^\circ \in \mathbb{R}^2$. Each anchor can range with each tag repeatedly. For the brevity of formulation, we consider repeatedly ranging for T times equivalent to deploying T anchors on the same site. In total, we have $M_T \triangleq MT$ anchors and $n = NM_T$ measurements.

We denote by d_{im} the measured distance from the m -th anchor to the i -th tag. The measurement model is as follows:

$$d_{im} = \|\mathbf{a}_m^\mathcal{A} - \mathbf{R}^\circ \mathbf{s}_i^\mathcal{B} - \mathbf{t}^\circ\| + r_{im} \quad (1)$$

where r_{im} is the additive measurement noise.

Assumption 1: r_{im} 's are i.i.d Gaussian noises with zero mean and finite and known standard deviation $\sigma_{im} > 0$.

The RBL problem is formulated as follows: given $\mathbf{a}_m^\mathcal{A}, \mathbf{s}_i^\mathcal{B}$ and the distance measurements d_{im} , estimate the pose of the rigid body, i.e., the rotation \mathbf{R}° and the position \mathbf{t}° .

B. Maximum Likelihood Formulation

The maximum likelihood estimate of the planar RBL problem is the solution to the following optimization problem:

$$(\text{ML}) \min_{\mathbf{R}, \mathbf{t}} \sum_{i=1}^N \sum_{m=1}^{M_T} \frac{(d_{im} - \|\mathbf{a}_m^\mathcal{A} - \mathbf{R} \mathbf{s}_i^\mathcal{B} - \mathbf{t}\|)^2}{\sigma_{im}^2} \quad (2a)$$

$$\text{s.t. } \mathbf{R} \in \text{SO}(2), \mathbf{t} \in \mathbb{R}^2, \quad (2b)$$

C. Squared Least Squares Formulation

We square both sides of (1) and have:

$$d_{im}^2 = (\|\mathbf{a}_m^\mathcal{A} - \mathbf{R} \mathbf{s}_i^\mathcal{B} - \mathbf{t}\| + r_{im})^2 \quad (3a)$$

$$\begin{aligned} &= \|\mathbf{a}_m^\mathcal{A}\|^2 - 2\mathbf{a}_m^\mathcal{A}{}^\top (\mathbf{R} \mathbf{s}_i^\mathcal{B} + \mathbf{t}) + \|\mathbf{R} \mathbf{s}_i^\mathcal{B} + \mathbf{t}\|^2 \\ &+ 2\|\mathbf{a}_m^\mathcal{A} - \mathbf{R} \mathbf{s}_i^\mathcal{B} - \mathbf{t}\| r_{im} + r_{im}^2 \end{aligned} \quad (3b)$$

From Assumption 1, we know that the noise term $\varepsilon_{im} := 2\|\mathbf{a}_m^\mathcal{A} - \mathbf{R} \mathbf{s}_i^\mathcal{B} - \mathbf{t}\| r_{im} + r_{im}^2$ in (3b) has mean σ_{im}^2 , we can subtract it from both sides of (3b) and have:

$$d_{im}^2 - \sigma_{im}^2 = \|\mathbf{a}_m^\mathcal{A}\|^2 - 2\mathbf{a}_m^\mathcal{A}{}^\top (\mathbf{R} \mathbf{s}_i^\mathcal{B} + \mathbf{t}) + \|\mathbf{R} \mathbf{s}_i^\mathcal{B} + \mathbf{t}\|^2 + e_{im}, \quad (4)$$

where $e_{im} = 2\|\mathbf{a}_m^\mathcal{A} - \mathbf{R} \mathbf{s}_i^\mathcal{B} - \mathbf{t}\| r_{im} + (r_{im}^2 - \sigma_{im}^2)$ has zero mean. Note that in earlier studies [16], [17], the chi-squared random variable r_{im}^2 is omitted. As shown in Section V, ignoring r_{im}^2 deteriorates the estimator's performance when σ_{im} is large.

¹<https://github.com/SLAMLab-CUHKSZ/Efficient-Pose-Estimation-via-UWB-measurements>

Stacking (4) over the measurements for i -th tag gives

$$\mathbf{d}_i = -2\mathbf{A}^\top(\mathbf{R}\mathbf{s}_i^{\mathcal{B}} + \mathbf{t}) + \|\mathbf{R}\mathbf{s}_i^{\mathcal{B}} + \mathbf{t}\|^2 \mathbf{1}_{M_T} + \mathbf{e}_i \quad (5)$$

where

$$\mathbf{A} = \begin{bmatrix} \mathbf{a}_1^{\mathcal{A}} & \mathbf{a}_2^{\mathcal{A}} & \dots & \mathbf{a}_{M_T}^{\mathcal{A}} \end{bmatrix} \in \mathbb{R}^{2 \times M_T} \quad \mathbf{S} = \begin{bmatrix} \mathbf{s}_1^{\mathcal{B}} & \mathbf{s}_2^{\mathcal{B}} & \dots & \mathbf{s}_N^{\mathcal{B}} \end{bmatrix} \in \mathbb{R}^{2 \times N}$$

$$\mathbf{d}_i = \begin{bmatrix} d_{i1}^2 - \|\mathbf{a}_1^{\mathcal{A}}\|^2 - \sigma_{i1}^2 \\ \vdots \\ d_{iM_T}^2 - \|\mathbf{a}_{M_T}^{\mathcal{A}}\|^2 - \sigma_{iM_T}^2 \end{bmatrix} \quad \text{and} \quad \mathbf{e}_i = \begin{bmatrix} e_{i1} \\ \vdots \\ e_{iM_T} \end{bmatrix}.$$

The squared least squares problem is formulated as follows:

$$\text{(SLS)} \min_{\mathbf{R}, \mathbf{t}} \sum_{i=1}^N \|\mathbf{d}_i + 2\mathbf{A}^\top(\mathbf{R}\mathbf{s}_i^{\mathcal{B}} + \mathbf{t}) - \|\mathbf{R}\mathbf{s}_i^{\mathcal{B}} + \mathbf{t}\|^2 \mathbf{1}_{M_T}\|_{\Sigma_{\mathbf{e}_i}}^2 \quad (6a)$$

$$\text{s.t. } \mathbf{R} \in \text{SO}(2), \quad \mathbf{t} \in \mathbb{R}^2, \quad (6b)$$

where $\|\cdot\|_{\Sigma}^2 \triangleq (\cdot)^\top \Sigma^{-1}(\cdot)$, and $\Sigma_{\mathbf{e}_i}$ is the covariance of \mathbf{e}_i .

Previous works differ in the way they deal with the quadratic term $\|\mathbf{R}\mathbf{s}_i^{\mathcal{B}} + \mathbf{t}\|^2$. The works [15], [16] multiply both sides of (5) by projection matrix or orthonormal basis of $\text{Null}(\mathbf{1})$ and formulate a linear LS problem, while [17] expands the quadratic term and formulate an SDP problem.

III. AN EFFICIENT PLANAR POSE ESTIMATOR

We devise the planar pose estimator in two steps. In section III-A, we design a computationally efficient consistent estimator. In section III-B, we refine the estimates by one step of the Gauss-Newton iteration. The two-step scheme has the unrivaled property as stated in the following theorem:

Theorem 1: Suppose that $\hat{\mathbf{R}}$ and $\hat{\mathbf{t}}$ are \sqrt{n} -consistent estimates of \mathbf{R}^0 and \mathbf{t}^0 . The estimates $\hat{\mathbf{R}}_{\text{GN}}, \hat{\mathbf{t}}_{\text{GN}}$ obtained by one step of Gauss-Newton iteration on problem 2 has the same asymptotic efficiency as the ML estimator in the sense that

$$\hat{\mathbf{R}}_{\text{GN}} - \hat{\mathbf{R}}_{\text{ML}} = o_p(\mathbf{1}/\sqrt{n}), \quad \hat{\mathbf{t}}_{\text{GN}} - \hat{\mathbf{t}}_{\text{ML}} = o_p(\mathbf{1}/\sqrt{n}),$$

The proof is given in Appendix A.

A. Unconstrained Least Squares Estimator

Denote the projection matrix onto $\text{Null}(\mathbf{1}_{M_T})$ as $\mathbf{P} = \mathbf{I}_{M_T} - (\mathbf{1}_{M_T} \mathbf{1}_{M_T}^\top) / M_T$. Multiply both sides of (5) by \mathbf{P} and eliminate the quadratic term, we formulate the following problem [15]:

$$\text{(PSLS)} \min_{\mathbf{R}, \mathbf{t}, \mathbf{n}} \sum_{i=1}^N \|\mathbf{P}\mathbf{d}_i + 2\mathbf{P}\mathbf{A}^\top(\mathbf{R}\mathbf{s}_i^{\mathcal{B}} + \mathbf{t})\|_{\Sigma_{\mathbf{e}_i}}^2 \quad (7a)$$

$$\text{s.t. } \mathbf{R} \in \text{SO}(2), \quad \mathbf{t} \in \mathbb{R}^2 \quad (7b)$$

where $\Sigma_{\mathbf{e}_i}$ is the covariance matrix for $\mathbf{P}\mathbf{e}_i$. The matrix $\Sigma_{\mathbf{e}_i}$ is dense and dependent on the true distance d_{im}^0 [15]. The works [15], [16] use the distance measurements d_{im} to approximate $\Sigma_{\mathbf{e}_i}$, but it can undermine the accuracy when σ_{im} is large.

The rotation matrix \mathbf{R} has a nice structure, such that we can parameterize \mathbf{R} by an angle $\theta \in [0, 2\pi)$:

$$\mathbf{R}(\theta) \triangleq \begin{bmatrix} \cos \theta & -\sin \theta \\ \sin \theta & \cos \theta \end{bmatrix}. \quad (8)$$

Motivated by (8), we can use a unit-length vector $\mathbf{y} \in \mathbb{R}^2$ to parameterize \mathbf{R} . Denote $\mathbf{A}\mathbf{P}$ as $\bar{\mathbf{A}}$, $\mathbf{P}\mathbf{d}_i$ as $\bar{\mathbf{d}}_i$, and $\mathbf{P}\mathbf{e}_i$ as $\bar{\mathbf{e}}_i$, we formulate the following GTRS problem:

$$\min_{\mathbf{y}, \mathbf{t}} \|\bar{\mathbf{d}} - \mathbf{H}_1 \Gamma \mathbf{y} - \mathbf{H}_2 \mathbf{t}\|_{\mathbb{R}^2}^2 \quad \text{s.t. } \|\mathbf{y}\|^2 = \mathbf{1} \quad (9)$$

where $\Gamma = \begin{bmatrix} 0 & 1 & -1 & 0 \\ 1 & 0 & 0 & 1 \end{bmatrix}^\top$, $\bar{\mathbf{d}} = (\bar{\mathbf{d}}_1, \dots, \bar{\mathbf{d}}_N)$,

$\mathbf{H}_1 = -2\mathbf{S}^\top \otimes \bar{\mathbf{A}}^\top$, and $\mathbf{H}_2 = -2\mathbf{1}_N \otimes \bar{\mathbf{A}}^\top$.

Although the work [19] provides a necessary and sufficient condition for the non-convex GTRS problem, the difficult singular case is not well studied [20]. Considering the computational efficiency and ease of proof, we discard the constraint and covariance and solve the LS problem. Considering the computational efficiency and ease of proof, we discard the constraint and covariance and solve the ordinary LS problem.

Lemma 1: Under Assumption 3, the design matrix $\mathbf{H} = [\mathbf{H}_1 \Gamma, \mathbf{H}_2]$ is full column rank, and the unique solution to the ordinary least squares problem is given by:

$$\text{(ULS)} \quad \begin{bmatrix} \hat{\mathbf{y}} \\ \hat{\mathbf{t}} \end{bmatrix} = (\mathbf{H}^\top \mathbf{H})^{-1} \mathbf{H}^\top \bar{\mathbf{d}}, \quad (10)$$

Theorem 2: The ULS estimator is \sqrt{n} -consistent, i.e.,

$$\begin{bmatrix} \hat{\mathbf{y}} \\ \hat{\mathbf{t}} \end{bmatrix} - \begin{bmatrix} \mathbf{y}^o \\ \mathbf{t}^o \end{bmatrix} = O_p(\mathbf{1}/\sqrt{n}).$$

The proof is given in Appendix B and C.

Before moving on to the second step, we notice that the estimate $\hat{\mathbf{y}}$ from (10) is not constrained to have unit length, thus we further project $\hat{\mathbf{R}} \triangleq \Gamma \hat{\mathbf{y}}$ onto $\text{SO}(2)$. The matrix projection π that maps an arbitrary matrix $\mathbf{X} \in \mathbb{R}^{2 \times 2}$ onto $\text{SO}(2)$ at a matrix $\mathbf{W} \in \text{SO}(2)$ is defined as

$$\pi(\mathbf{X}) = \arg \min_{\mathbf{W} \in \text{SO}(2)} \|\mathbf{X} - \mathbf{W}\|_F^2. \quad (11)$$

Let the SVD of \mathbf{X} be $\mathbf{U}\Sigma\mathbf{V}^\top$, we have

$$\pi(\mathbf{X}) = \mathbf{U} \text{diag}([1, \det(\mathbf{U}\mathbf{V}^\top)]) \mathbf{V}^\top \quad (12)$$

Theorem 3: The projected estimate generated by (11) is \sqrt{n} -consistent, i.e., $\pi(\hat{\mathbf{R}}) - \mathbf{R}^0 = O_p(\mathbf{1}/\sqrt{n})$.

The proof is given in Appendix D.

B. One Step of the Gauss-Newton Iteration

Given a \sqrt{n} -consistent estimate from the first step, we implement one step of Gauss-Newton iteration on the **ML** problem (2) and obtain the **GN-ULS** estimator. Using (8), we can transform problem (2) into an unconstrained one:

$$\min_{\theta, \mathbf{t}} \sum_{i=1}^N \sum_{m=1}^{M_T} \frac{(d_{im} - \|\mathbf{a}_m^{\mathcal{A}} - \mathbf{L}_i \text{vec}(\mathbf{R}(\hat{\theta} + \theta)) - \mathbf{t}\|)^2}{\sigma_{im}^2} \quad (13)$$

where $\mathbf{L}_i = (\mathbf{s}_i^{\mathcal{B}} \otimes \mathbf{I}_2)^\top \in \mathbb{R}^{2 \times 4}$ and $\mathbf{R}(\hat{\theta}) = \pi(\hat{\mathbf{R}})$.

We use $\theta = 0, \mathbf{t} = \hat{\mathbf{t}}$ as the initial value. Write $f_{im}(\theta, \mathbf{t}) \triangleq \mathbf{a}_m^{\mathcal{A}} - \mathbf{L}_i \text{vec}(\mathbf{R}(\hat{\theta} + \theta)) - \mathbf{t}$ and $f_{im}^{(0)} \triangleq f_{im}(0, \hat{\mathbf{t}})$. The derivatives of $\|f_{im}(\theta, \hat{\mathbf{t}})\|$ w.r.t θ and \mathbf{t} are:

$$\frac{\partial \|f_{im}(0, \hat{\mathbf{t}})\|}{\partial(\theta, \mathbf{t})} = \begin{bmatrix} -\frac{1}{\|f_{im}^{(0)}\|} \Psi^\top (\mathbf{I}_2 \otimes \hat{\mathbf{R}}^\top) \mathbf{L}_i^\top f_{im}^{(0)} \\ -\frac{1}{\|f_{im}^{(0)}\|} f_{im}^{(0)} \end{bmatrix}$$

where $\Psi = \frac{\partial \text{vec}(\mathbf{R}(0))}{\partial \theta} = [0 \ 1 \ -1 \ 0]^\top$. Stacking the rows $\frac{\partial \|f_{im}(0, \hat{\mathbf{t}})\|}{\partial (\theta, \hat{\mathbf{t}})}$ gives the matrix \mathbf{J}_0 . Stacking $\|f_{im}^{(0)}\|$ gives the vector $\mathbf{f}(0, \hat{\mathbf{t}})$. Denote the covariance matrix of r_{im} as Σ_n , the one step of Gauss-Newton iteration $(\hat{\theta}, \hat{\mathbf{t}})_{\text{GN}}$ writes:

$$(\hat{\theta}, \hat{\mathbf{t}})_{\text{GN}} = (0, \hat{\mathbf{t}}) + (\mathbf{J}_0^\top \Sigma_n^{-1} \mathbf{J}_0)^{-1} \mathbf{J}_0^\top \Sigma_n^{-1} (\mathbf{d} - \mathbf{f}(0, \hat{\mathbf{t}})) \quad (14)$$

as such, we obtain the **GN-ULS** estimates,

$$(\text{GN-ULS}) \quad \hat{\mathbf{R}}_{\text{GN}} = \mathbf{R}(\hat{\theta} + \hat{\theta}_{\text{GN}}), \quad \hat{\mathbf{t}}_{\text{GN}} = \hat{\mathbf{t}}_{\text{GN}} \quad (15)$$

We summarize the **GN-ULS** estimator in Algorithm 1.

Algorithm 1 Unconstrained Least Squares estimator refined by one-step of Gauss-Newton iteration (GN-ULS)

Require: assumption 3 satisfied.

Input: $d_{im}, \sigma_{im}, \mathbf{a}_m^{\mathcal{A}}$ and $\mathbf{s}_i^{\mathcal{B}}$.

Output: the estimates of \mathbf{R}^o and \mathbf{t}^o .

- 1: Construct $\bar{\mathbf{d}} \in \mathbb{R}^{n \times 1}$ and $\mathbf{H} \in \mathbb{R}^{n \times 4}$.
 - 2: Derive the **ULS** estimator as $(\mathbf{H}^\top \mathbf{H})^{-1} \mathbf{H}^\top \bar{\mathbf{d}}$.
 - 3: Project the **ULS** estimate onto $SO(2)$ (11).
 - 4: Construct $\mathbf{J}_0^\top \in \mathbb{R}^{n \times 3}$ and $\mathbf{f}(0, \hat{\mathbf{t}}) \in \mathbb{R}^{n \times 1}$.
 - 5: Implement one step Gauss-Newton iteration (14).
 - 6: Obtain the **GN-ULS** estimator (15).
-

IV. ASYMPTOTIC EFFICIENCY CONDITIONS

According to Theorem 1, the **GN-ULS** estimates converge to the ML estimates $\hat{\mathbf{R}}_{\text{ML}}$ and $\hat{\mathbf{t}}_{\text{ML}}$ as the measurement number n increases. In this section, we give conditions related to anchor geometry, under which the ML estimator, therefore the **GN-ULS** estimator, is asymptotically efficient. We consider the case where the measurement number n increases from ranging repeatedly or deploying new anchors. Similar results can be derived when measurement number n increases from deploying new tags.

Assumption 2: The sample distribution F_m of the sequence $\mathbf{a}_1^{\mathcal{A}}, \mathbf{a}_2^{\mathcal{A}}, \dots$ converges to some distribution F_μ .

Example 1: Suppose $\mathbf{a}_m^{\mathcal{A}}$'s are independent samples from distribution function F_μ , F_m converges to F_μ as M increases.

Example 2: As the number T of repeated ranging increases, F_m converges to F_μ . Denote the measure induced by F_μ as μ , we have $\mu(\mathbf{a}_m^{\mathcal{A}}) = \frac{1}{M}$ for $m = 1, \dots, M$.

Assumption 3: There exist at least three non-colinear anchors and at least two tags non-colinear with the origin $O^{\mathcal{B}}$ of the local reference frame.

Assumption 4: Consider the limit measure μ in Assumption 2, there does not exist any line \mathcal{L} such that $\mu(\mathcal{L}) = 1$.

Theorem 4: Under assumptions 2-4, the **ML** estimates, therefore the **GN-ULS** estimates are asymptotically efficient, i.e., as measurement number n increases,

$$\begin{aligned} (\text{vec}(\hat{\mathbf{R}}_{\text{ML}}, \hat{\mathbf{t}}_{\text{ML}}) &\sim \mathcal{N}((\text{vec}(\mathbf{R}^o), \mathbf{t}^o), \text{CRLB}), \\ (\text{vec}(\hat{\mathbf{R}}_{\text{GN}}, \hat{\mathbf{t}}_{\text{GN}}) &\sim \mathcal{N}((\text{vec}(\mathbf{R}^o), \mathbf{t}^o), \text{CRLB}). \end{aligned}$$

The proof is given in Appendix E, and the derivation of CRLB is given in Appendix F.

Remark 1: In practice, the significance of Theorem 4 is that it gives the theoretical covariance of **GN-ULS** estimates,

that is, the CRLB. Note that determining the covariance of pose estimates is vital in sensor fusion and is generally not trivial. Although we need the true pose $\mathbf{R}^o, \mathbf{t}^o$ to calculate CRLB, we can reasonably use $\hat{\mathbf{R}}_{\text{GN}}, \hat{\mathbf{t}}_{\text{GN}}$ to approximate it.

V. SIMULATIONS AND DISCUSSIONS

We verify the asymptotic efficiency of the proposed **GN-ULS** estimator by comparing the root mean square error (RMSE) with the lower bound, which is the square root of the trace of CRLB [15], denoted as $\sqrt{\text{CRLB}}$. We also compare **GN-ULS** with previous works [16] and [17], denoted as the **GTRS** and the **GN-SDP** estimator respectively.

A. Simulation Setup

In our simulations, the rigid body is a square with a side length of 3 meters, and the environment space is a square with a side length of 50 meters. There are $M = 3$ anchors deployed at $[50, 0]^\top$, $[50, 50]^\top$ and $[0, 50]^\top$. There are $N = 2$ tags deployed at $[3, 0]^\top$ and $[3, 3]^\top$ in the local frame. The true pose is $\mathbf{t}^o = [0, 25]^\top$ and the rotation angle is $\theta^o = 60^\circ$.

For each setting, we run $L = 1000$ Monte-Carlo experiments and report the average results. We use the chordal distance [21] to calculate the RMSE for the rotation matrix:

$$\text{RMSE}(\mathbf{R}) = \sqrt{\frac{1}{L} \sum_{l=1}^L \|\hat{\mathbf{R}} - \mathbf{R}^o\|_F^2}$$

B. Simulation Results

1) *Asymptotic efficiency under repeated ranging:* We study the asymptotic efficiency by increasing the number T of repeated ranging. The noise standard deviation σ_{mi} 's are set to be 0.05[1, 2, 3, 4, 5, 6]. As shown in Fig. 2a, the **UCLS** estimator is consistent but not asymptotically efficient, but one step of Gauss-Newton iteration is sufficient to achieve the accuracy lower bound. The **GTRS** estimator deviates from the lower bound under large samples, the reason is twofold. First, the chi-squared random variable r_{im}^2 is omitted in (3b). Second, the estimate is refined on the **SLS** problem but not on the **ML** problem (2). In contrast, although the **GN-SDP** estimator also omits r_{im}^2 , it refines the estimates on (2) and achieves the lower bound. Both **GN-SDP** and **GTRS** estimators are computationally more complex than **GN-ULS** as shown in Figure. 2b. The worst-case complexity of **GN-SDP** is $O(n^2)$ [17]. Both **GN-ULS** and **GTRS** have $O(n)$ complexity [16], but **GTRS** involves more computation for considering the constraint and covariance.

2) *Asymptotic efficiency under numerous anchors:* We study the asymptotic performance by deploying new anchors. The standard deviation σ_{im} is set to be 0.1, and we deploy new anchors whose positions follow the uniform distribution on the simulation plane. As shown in Fig. 3a, the **GTRS** estimator deviates from the lower bound due to the same reasons discussed above. When we deploy 10000 anchors, the MATLAB CVX toolbox reports the SDP problem as infeasible, and the **GN-SDP** estimator fails. The same instability problem occurs in Trial 3 when σ_{im} 's are small.

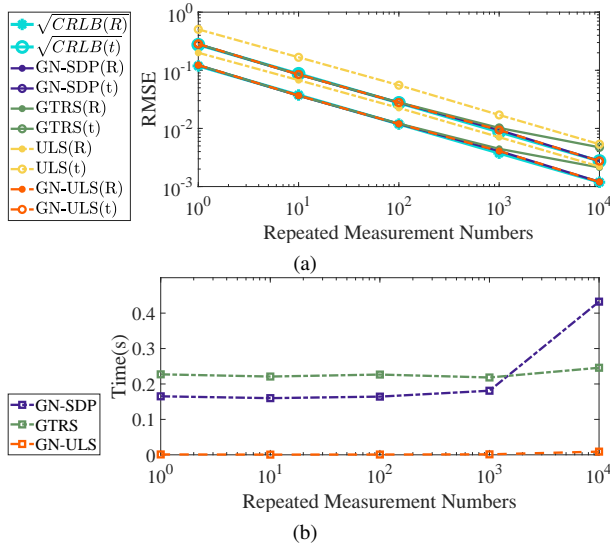


Fig. 2: Performance under repeated ranging. (a) RMSE of different pose estimators and the lower bound as the number T of repeated ranging increases. (b) Computation time of different pose estimators as T increases.

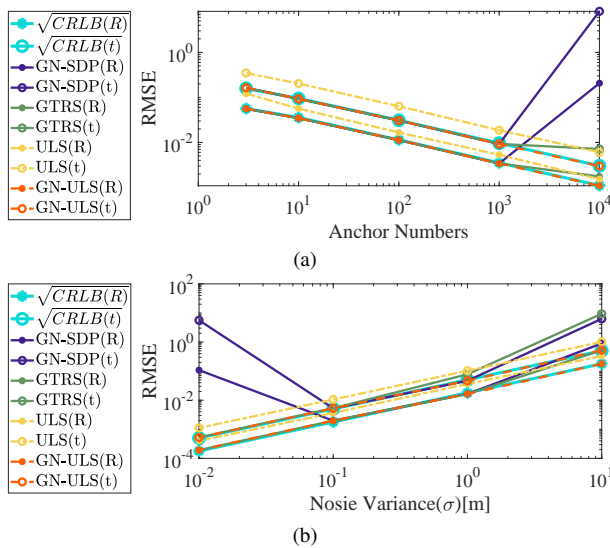


Fig. 3: Performance with numerous anchors and under different noise levels. (a) RMSE of different pose estimators and the lower bound when the number M of anchors increases. (b) RMSE of different pose estimators and the lower bound as the standard deviation increases.

3) *Asymptotic efficiency under large noise*: We study the asymptotic performance under large standard deviations. We adjust the standard deviation σ_{im} from 0.01 to 10, and set $T = 1000$. As shown in Fig. 3b, **GTRS** and **GN-SDP** deviate from the lower bound over large σ , this is because they omit r_{im}^2 in (3b) and use noisy measurements to approximate the covariance matrix. The results imply that if the initial estimate is not consistent, a one-step of Gauss-Newton iteration is not sufficient to yield an asymptotically efficient estimate, validating Theorem 1 from another perspective.

C. Discussions

As the simulation results indicate, the **GN-ULS** attains lower bound accuracy, i.e., \sqrt{CRLB} , and performs better than computationally more complex estimators in stability and accuracy under large noise. The key insight is to construct a \sqrt{n} -consistent estimator in the first step as computationally efficient as possible and further ameliorate the estimate on the **ML** problem rather than the **SLS** problem.

VI. EXPERIMENTS

In this section, we introduce data collection and present experimental results on static and dynamic datasets.

A. System Overview

Fig. 4 presents the experimental system and environment with an overall volume of $10m \times 6m \times 4m$. The system consists of a motion capture system (OptiTrack: X22), UWB (NoopLoop: LinkTrack), an Ackerman trolley platform, and an embedded processor (NVIDIA: TX2). The rigid body is a carbon fiber cube frame attached to the trolley. Three UWB tags are fixed on the cube at the same height as the eight anchors deployed in the environment.

B. Data Collection

We refer to the motion capture frame as the global frame. The UWB ranging frequency is 100Hz, and the motion capture system provides the ground truth of the pose at 120Hz. During experiments, NVIDIA-TX2 unpacks the UWB data through its serial port and collects the motion capture system data through TCP. In dynamic datasets, we synchronize measurements using the system time of TX2 and perform interpolation to align the motion capture measurements with the UWB measurements. The synchronization is not perfect due to processing delay. Thus, in experiments we further align the estimate and truth based on localization error.

C. UWB Calibration

UWB ranging measurement is practically modeled as:

$$\hat{d} = d^o + f(d^o) + e, \quad (16)$$

where $f(d^o)$ is a distance-related bias, and e is a zero-mean Gaussian noise. We quiescent the trolley for a period of time and use the sample variance to estimate the standard deviation of e . The more demanding task is to calibrate $f(d^o)$, which we assume to be a linear function of d^o [22]. We control the trolley to move around in the environment, collect

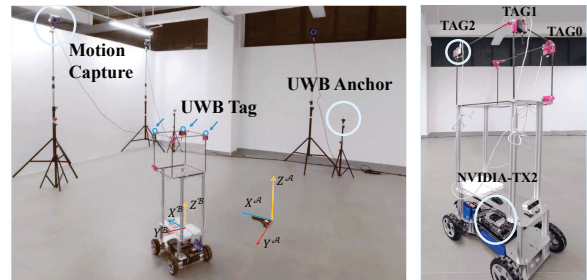


Fig. 4: Experiment Setup

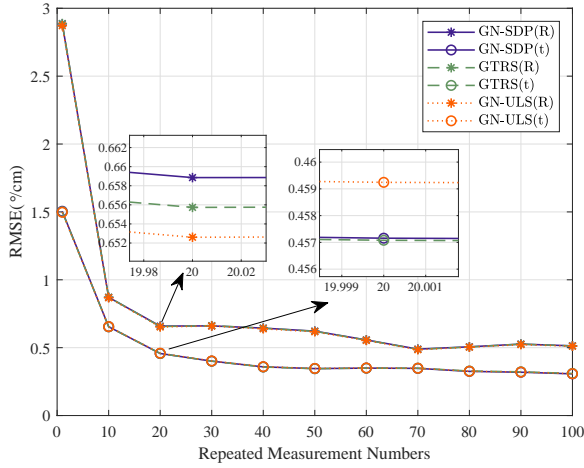


Fig. 5: Static experiment under repeated ranging

calibration datasets and use the least squares method to fit $f(d^o)$. Considering the complex communication environment indoors, we implement outlier rejection before calibration. Similar to the methods in [8], [10], a range measurement at instant t is rejected as an outlier if

$$d_t > \min\{d_{t-k}, \dots, d_{t-1}\} + \frac{kv_{\max}}{f} + 0.1, \quad (17)$$

where k is the length of the time window, v_{\max} is the velocity upper bound during the experiment, f is the ranging frequency, and $0.1m$ is a general error bound of UWB.

D. Static Datasets and Pose Estimation Results

We place the trolley at different sites and change the orientation from 0° to 300° at an interval of approximately 60° . In total, we collect 42 static datasets, each lasting for around 100 seconds. On these static datasets, we investigate the asymptotic performance of different estimators. We obtain the RMSE on all the poses and compare the average result.

We choose two tags and three anchors and use the centimeter and the degree as units for Fig. 5. The result shows that **GN-ULS** attains millimeter and sub-degree accuracy using ten rounds of range measurements.

E. Dynamic Datasets and Pose Estimation Results

In the dynamic datasets, we control the trolley to move at different speeds and collect fast, medium, and slow datasets. The average speed are respectively 0.49m/s, 0.23m/s and 0.11m/s. we conduct interpolation to fill in the range measurements when outliers occur. We can not utilize repeated measurements in the dynamic case. Instead, we use measurements from all three tags and eight anchors to improve accuracy. Fig. 6 presents the results on the fast dataset, where our method achieves an average RMSE of 7.28° and $2.74cm$ using one round ranging measurements between eight anchors and three tags. The overall results of three datasets are summarized in Table I.

F. Discussions

In our static and dynamic datasets, **GN-ULS**, **GN-SDP** and **GTRS** achieve almost the same accuracy. The reason is

TABLE I: Position and Rotation RMSE on dynamic datasets

Method	Position RMSE [cm]			Rotation RMSE[deg]		
	Fast	Mid	Slow	Fast	Mid	Slow
ULS	3.5410	34869	3.3521	7.6459	7.4194	8.1393
GN-ULS	2.7432	2.7294	2.4188	7.2846	7.0606	8.0560
GN-SDP	2.7394	2.7250	2.4133	7.2104	7.0220	8.0122
GTRS	2.8789	2.8208	2.5500	7.0745	7.1374	8.3082

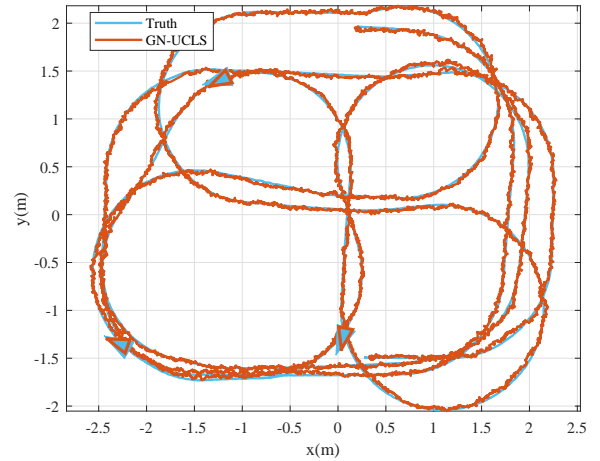


Fig. 6: Dynamic experiment on the fast dataset

that the standard deviation σ is very small in experiments, in the magnitude of 10^{-2} . The main advantage of **GN-ULS** is computational efficiency. Table. II presents the computation time of different estimators as the number n of measurements increases, the results indicate that only **ULS** and **GN-ULS** can provide pose estimate in real time. We believe that our method should have a considerable advantage in real-time and high-speed scenarios.

The estimators' performance is not as good on the dynamic datasets as on the static datasets, the main reason is the complex indoor environment, where the distance-related bias $f(d^o)$ varies at different positions and orientations due to obstruction and the multi-path effect.

TABLE II: Computation Time

Method	Average Computation Time[s]		
	n=6	n=600	n=60000
ULS	0.0007	0.0007	0.0078
GN-ULS	0.0008	0.0009	0.0113
GN-SDP	0.1824	0.1939	0.4689
GTRS	0.2427	0.2497	0.2607

VII. CONCLUSION AND FUTURE WORK

This paper studies planar pose estimation using UWB range measurements. Grounded on a two-step architecture, we design an asymptotically efficient pose estimator **GN-ULS**. The proposed estimator defeats previous works in computational efficiency, stability and accuracy under large noise variance. In this work, we intend to present the possibility of using only range measurements for real-time pose estimation, thus we do not integrate motion models or

odeometry measurements which can smooth the trajectory and further improve the accuracy. In future work, we plan to combine onboard sensors such as IMU, Lidars and cameras.

APPENDIX A PROOF OF THEOREM 1

Proof: Consider problem (13) and we have \sqrt{n} -consistent estimates $\mathbf{R}(\hat{\theta}), \hat{\mathbf{t}}$. For simplicity, we omit the covariance matrix Σ_n in the proof. The optimal solution to (13) is $\theta^* = \ln(\mathbf{R}(\hat{\theta})^\top \hat{\mathbf{R}}_{\text{ML}})^\vee$ and $\mathbf{t}^* = \hat{\mathbf{t}}_{\text{ML}}$, where $\ln(\cdot)^\vee$ is the inverse map of (8). θ^* and \mathbf{t}^* should satisfy the first order condition:

$$\frac{1}{n} \mathbf{J}(\theta^*, \mathbf{t}^*)^\top (\mathbf{d} - \mathbf{f}(\theta^*, \mathbf{t}^*)) = \mathbf{0}$$

Apply order-one Taylor expansion around $(0, \hat{\mathbf{t}})$ yields:

$$\frac{1}{n} \mathbf{J}_0^\top (\mathbf{d} - \mathbf{f}(0, \hat{\mathbf{t}})) + \mathbf{G} \begin{bmatrix} \theta^* - 0 \\ \mathbf{t}^* - \hat{\mathbf{t}} \end{bmatrix} + o \left[\begin{bmatrix} \theta^* - 0 \\ \mathbf{t}^* - \hat{\mathbf{t}} \end{bmatrix} \right] = \mathbf{0}$$

where

$$\mathbf{G} = -\frac{1}{n} \mathbf{J}_0^\top \mathbf{J}_0 + \frac{1}{n} \sum_{i=1}^N \sum_{m=1}^{M_T} \frac{\partial^2 \|f_{im}^0\|}{\partial(\theta, \mathbf{t}) \partial(\theta, \mathbf{t})^\top} (d_{im} - \|f_{im}^{(0)}\|)$$

Given that $\mathbf{R}(\hat{\theta}), \mathbf{t}$ are consistent estimators of $\mathbf{R}^o, \mathbf{t}^o$ and Assumption 2 holds, we can apply central limit theorem and further writes:

$$\begin{aligned} \mathbf{G} &= -\frac{1}{n} \mathbf{J}_0^\top \mathbf{J}_0 + o_p(\mathbf{1}) \\ &= \mathbf{G}^o + O_p\left(\frac{1}{\sqrt{n}}\right) + o_p(\mathbf{1}) \end{aligned}$$

$$\mathbf{G}^o = \frac{1}{N} \sum_{i=1}^N \mathbb{E}_{\mathbf{a}^{\mathcal{A}} \sim \mu} \left(\frac{\partial \|\mathbf{a}^{\mathcal{A}} - \mathbf{L}_i \text{vec}(\mathbf{R}^o) - \mathbf{t}^o\|}{\partial(\theta, \mathbf{t})} \frac{\partial \|\mathbf{a}^{\mathcal{A}} - \mathbf{L}_i \text{vec}(\mathbf{R}^o) - \mathbf{t}^o\|}{\partial(\theta, \mathbf{t})} \right)$$

where $\mathbb{E}_{\mathbf{a}^{\mathcal{A}} \sim \mu}$ is taken over $\mathbf{a}^{\mathcal{A}}$ with respect to μ .

By matrix inversion lemma, we can prove that

$$\begin{aligned} \mathbf{G}^{-1} &= \left(-\frac{1}{n} \mathbf{J}_0^\top \mathbf{J}_0\right)^{-1} + o_p(\mathbf{1}) \\ \mathbf{G}^{-1} &= (\mathbf{G}^o)^{-1} + O_p\left(\frac{1}{\sqrt{n}}\right) + o_p(\mathbf{1}) \end{aligned}$$

Because

$$\begin{bmatrix} \theta^* - 0 \\ \mathbf{t}^* - \hat{\mathbf{t}} \end{bmatrix} = \begin{bmatrix} \theta_{\text{ML}} - \theta^0 + \theta^0 - \hat{\theta} \\ \mathbf{t}^* - \hat{\mathbf{t}} \end{bmatrix} = O_p\left(\frac{1}{\sqrt{n}}\right)$$

We have

$$\begin{aligned} \frac{1}{n} \mathbf{J}_0^\top (\mathbf{d} - \mathbf{f}(0, \hat{\mathbf{t}})) &= -\mathbf{G} \begin{bmatrix} \theta^* - 0 \\ \mathbf{t}^* - \hat{\mathbf{t}} \end{bmatrix} + o_p\left(\frac{1}{\sqrt{n}}\right) \\ &= -\mathbf{G}^o O_p\left(\frac{1}{\sqrt{n}}\right) + O_p\left(\frac{1}{n}\right) + o_p\left(\frac{1}{\sqrt{n}}\right) \\ &= O_p\left(\frac{1}{\sqrt{n}}\right) \end{aligned}$$

$$\begin{aligned} \begin{bmatrix} \theta^* \\ \mathbf{t}^* \end{bmatrix} &= \begin{bmatrix} 0 \\ \mathbf{t} \end{bmatrix} - \mathbf{G}^{-1} \frac{1}{n} \mathbf{J}_0^\top (\mathbf{d} - \mathbf{f}(0, \hat{\mathbf{t}})) + \mathbf{G}^{-1} o_p\left(\frac{1}{\sqrt{n}}\right) \\ &= \begin{bmatrix} 0 \\ \mathbf{t} \end{bmatrix} + \left(\frac{1}{n} \mathbf{J}_0^\top \mathbf{J}_0\right)^{-1} \frac{1}{n} \mathbf{J}_0^\top (\mathbf{d} - \mathbf{f}(0, \hat{\mathbf{t}})) \\ &\quad + \frac{1}{n} \mathbf{J}_0^\top (\mathbf{d} - \mathbf{f}(0, \hat{\mathbf{t}})) o_p(\mathbf{1}) + \mathbf{G}^{-1} o_p\left(\frac{1}{\sqrt{n}}\right) \\ &= \begin{bmatrix} \hat{\theta}_{\text{GN}} \\ \hat{\mathbf{t}}_{\text{GN}} \end{bmatrix} + o_p\left(\frac{1}{\sqrt{n}}\right) \end{aligned}$$

It follows then

$$\begin{aligned} \hat{\mathbf{t}}_{\text{GN}} &= \hat{\mathbf{t}}_{\text{ML}} + o_p\left(\frac{1}{\sqrt{n}}\right) \\ \hat{\mathbf{R}}_{\text{GN}} &= \mathbf{R}(\hat{\theta} + \theta^* + o_p\left(\frac{1}{\sqrt{n}}\right)) = \hat{\mathbf{R}}_{\text{ML}} + o_p\left(\frac{1}{\sqrt{n}}\right) \end{aligned}$$

■

APPENDIX B PROOF OF LEMMA 1

Given three non-colinear anchors and two tags non-colinear with the origin of local reference frame, we prove that $\mathbf{H} = [\mathbf{H}_1 \Gamma, \mathbf{H}_2]$ is full column rank.

Proof: Write \mathbf{H} as

$$\mathbf{H} = [-2\mathbf{S}^\top \otimes \bar{\mathbf{A}}^\top, -2\mathbf{1}_2 \otimes \bar{\mathbf{A}}^\top] \begin{bmatrix} \Gamma & \mathbf{0} \\ \mathbf{0} & \mathbf{I}_2 \end{bmatrix}$$

Here $\bar{\mathbf{A}} = \mathbf{A}\mathbf{P}$, and \mathbf{P} is the projection matrix onto $\text{Null}(\mathbf{1}_3)$. Multiplying \mathbf{A} by \mathbf{P} essentially subtract the average of anchor positions such that $\bar{\mathbf{A}}\mathbf{1}_3 = \mathbf{0}$. Because we assume the three anchors are non-colinear, we have $\text{rank}(\bar{\mathbf{A}}) = 2$. Using the property $\text{rank}(\mathbf{A} \otimes \mathbf{B}) = \text{rank}(\mathbf{A}) \times \text{rank}(\mathbf{B})$, we have $\text{rank}(\mathbf{H}_1) = \text{rank}(\mathbf{S}^\top) \times \text{rank}(\bar{\mathbf{A}}^\top) = 4$, and $\text{rank}([\mathbf{H}_1, \mathbf{H}_2]) = \text{rank}([\mathbf{S}^\top, \mathbf{1}_2]) \times \text{rank}(\bar{\mathbf{A}}^\top) = 4$. Thus, \mathbf{H}_2 can be written as $\mathbf{H}_1 \mathbf{C}$, where $\mathbf{C} \in \mathbb{R}^{4 \times 2}$ is the column transformation matrix. We can then write:

$$\mathbf{H} = \mathbf{H}_1 [\mathbf{I}_4, \mathbf{C}] \begin{bmatrix} \Gamma & \mathbf{0} \\ \mathbf{0} & \mathbf{I}_2 \end{bmatrix}$$

Because \mathbf{H}_1 is full column rank, to prove \mathbf{H} is full column rank, it suffices to prove $[\mathbf{I}_4, \mathbf{C}] \begin{bmatrix} \Gamma & \mathbf{0} \\ \mathbf{0} & \mathbf{I}_2 \end{bmatrix}$ is full rank. Next, we derive the formula for \mathbf{C} .

Because \mathbf{S}^\top is full rank, we can write $\mathbf{1}_2 = \mathbf{S}^\top \begin{bmatrix} \alpha \\ \beta \end{bmatrix}$ for some α and β , and $[\alpha, \beta]^\top$ is not a zero vector. Using the property $(\mathbf{A} \otimes \mathbf{B})(\mathbf{C} \otimes \mathbf{D}) = (\mathbf{A}\mathbf{C} \otimes \mathbf{B}\mathbf{D})$, we can write

$$\begin{aligned} \mathbf{H}_2 &= -2\mathbf{1}_2 \otimes \bar{\mathbf{A}}^\top = -2(\mathbf{S}^\top \begin{bmatrix} \alpha \\ \beta \end{bmatrix}) \otimes (\bar{\mathbf{A}}^\top \mathbf{I}_2) \\ &= -2(\mathbf{S}^\top \otimes \bar{\mathbf{A}}^\top) \left(\begin{bmatrix} \alpha \\ \beta \end{bmatrix} \otimes \mathbf{I}_2 \right) \end{aligned}$$

Thus we have

$$\mathbf{C} = \left(\begin{bmatrix} \alpha \\ \beta \end{bmatrix} \otimes \mathbf{I}_2 \right) = \begin{bmatrix} \alpha & 0 & \beta & 0 \\ 0 & \alpha & 0 & \beta \end{bmatrix}^\top$$

We end the proof by noticing that

$$[\mathbf{I}_4, \mathbf{C}] \begin{bmatrix} \Gamma & \mathbf{0} \\ \mathbf{0} & \mathbf{I}_2 \end{bmatrix} = \begin{bmatrix} 0 & 1 & \alpha & 0 \\ 1 & 0 & 0 & \alpha \\ -1 & 0 & \beta & 0 \\ 0 & 1 & 0 & \beta \end{bmatrix}$$

is full rank. \blacksquare

APPENDIX C PROOF OF THEOREM 2

The proof is supported by the following lemma.

Lemma 2: Let $\{X_k\}$ be a stationary sequence with $\mathbb{E}[X_k] = 0$ and $\mathbb{E}[X_k^2] \leq \infty$ for all k . It holds that $\sum_{k=1}^n X_k/\sqrt{n} = O_p(1)$. The proof of this lemma is straightforward using the Chebyshev's inequality.

Proof: Write $\begin{bmatrix} \hat{\mathbf{y}} \\ \hat{\mathbf{t}} \end{bmatrix}$ as $(\frac{1}{n}\mathbf{H}^\top\mathbf{H})^{-1}\frac{1}{n}\mathbf{H}^\top\bar{\mathbf{d}}$, and substitute

$$\bar{\mathbf{d}} = \mathbf{H} \begin{bmatrix} \mathbf{y}^o \\ \mathbf{t}^o \end{bmatrix} + \begin{bmatrix} \bar{\mathbf{e}}_1 \\ \vdots \\ \bar{\mathbf{e}}_N \end{bmatrix}, \text{ we have:}$$

$$\begin{bmatrix} \hat{\mathbf{y}} \\ \hat{\mathbf{t}} \end{bmatrix} = \begin{bmatrix} \mathbf{y}^o \\ \mathbf{t}^o \end{bmatrix} + (\frac{1}{n}\mathbf{H}^\top\mathbf{H})^{-1}O_p(\mathbf{1}/\sqrt{n}).$$

The second term is from Lemma 2 and can be further written as $O_p(\mathbf{1}/\sqrt{n})$ when $(\frac{1}{n}\mathbf{H}^\top\mathbf{H})^{-1}$ converges under assumptions in Section IV. \blacksquare

APPENDIX D PROOF OF THEOREM 3

Proof: For any $\hat{\mathbf{R}}$, we can verify that

$$\|\pi(\hat{\mathbf{R}}) - \mathbf{R}^o\|_F \leq \|\pi(\hat{\mathbf{R}}) - \hat{\mathbf{R}}\|_F + \|\hat{\mathbf{R}} - \mathbf{R}^o\|_F \leq 2\|\hat{\mathbf{R}} - \mathbf{R}^o\|_F$$

Notice that $\|\hat{\mathbf{R}} - \mathbf{R}^o\|_F = \|\Gamma(\hat{\mathbf{y}} - \mathbf{y}^o)\|_2$, and $\hat{\mathbf{y}} - \mathbf{y}^o = O_p(\mathbf{1}/\sqrt{n})$, we conclude that each entry of $\pi(\hat{\mathbf{R}}) - \mathbf{R}^o$ should be $O_p(\mathbf{1}/\sqrt{n})$, i.e., $\pi(\hat{\mathbf{R}})$ is \sqrt{n} -consistent. \blacksquare

APPENDIX E PROOF OF THEOREM 4

Let $\Theta = (\text{vec}(\mathbf{R}), \mathbf{t})$ be the unknown parameter vector. First, we will show that the ML solution $\hat{\Theta}_{M_T}^{\text{ML}}$ that optimally solves problem (2) is consistent. Before that, we define two functions on real sequences.

Definition 1: Let $\mathbf{p} \triangleq (p_i)_{i \in \mathbb{N}}$ and $\mathbf{q} \triangleq (q_i)_{i \in \mathbb{N}}$ be two sequences of real numbers, if $t^{-1}\sum_{i=1}^t p_i q_i$ converges to a real number, we call its limit, denoted as $\langle \mathbf{p}, \mathbf{q} \rangle_t$, the tail product of \mathbf{p} and \mathbf{q} . We call $\|\mathbf{p}\|_t \triangleq \sqrt{\langle \mathbf{p}, \mathbf{p} \rangle_t}$, if it exists, the tail norm of \mathbf{p} .

Define $\mathbf{d}^o(\Theta) \triangleq (d_j^o(\Theta))_{j=1}^\infty$, where $d_j^o(\Theta) = \|\mathbf{a}_m^{\mathcal{A}} - \bar{\mathbf{L}}_i \Theta\|/\sigma_{im}$, $\bar{\mathbf{L}}_i = [\mathbf{L}_i, \mathbf{I}_2] \in \mathbb{R}^{2 \times 6}$ and $j = (m-1)N + i$. Note that $d_j^o(\Theta)$ is continuous with respect to $\mathbf{a}_m^{\mathcal{A}}$ and is bounded when $\mathbf{a}_m^{\mathcal{A}}$ is bounded. Then given Assumption 2, the tail norm $\|\mathbf{d}^o(\Theta) - \mathbf{d}^o(\Theta^o)\|_t^2$ exists by using the Helly-Bray theorem [23].

Next, we will show that under Assumption 3 and 4, the function $\|\mathbf{d}^o(\Theta) - \mathbf{d}^o(\Theta^o)\|_t^2$ has a unique minimum at $\Theta = \Theta^o$. By definition, we have $\|\mathbf{d}^o(\Theta) - \mathbf{d}^o(\Theta^o)\|_t^2$ equals

$$\frac{1}{N} \sum_{i=1}^N \mathbb{E}_{\mathbf{a}^{\mathcal{A}} \sim \mu} \left[\left(\|\mathbf{a}^{\mathcal{A}} - \bar{\mathbf{L}}_i \Theta\| - \|\mathbf{a}^{\mathcal{A}} - \bar{\mathbf{L}}_i \Theta^o\| \right)^2 \right],$$

where $\mathbb{E}_{\mathbf{a}^{\mathcal{A}} \sim \mu}$ is taken over $\mathbf{a}^{\mathcal{A}}$ with respect to μ .

It is straightforward that when the tags are not colinear with the origin of local reference frame, for any $\Theta \neq \Theta^o$, there exists an \mathbf{s}_i such that $\bar{\mathbf{L}}_i \Theta \neq \bar{\mathbf{L}}_i \Theta^o$. Suppose there exists a $\Theta \neq \Theta^o$ such that $\|\mathbf{d}^o(\Theta) - \mathbf{d}^o(\Theta^o)\|_t^2 = 0$. Then we have $\mu(\mathcal{A}_{\Theta, \mathbf{s}_i}) = 1$, where $\mathcal{A}_{\Theta, \mathbf{s}_i} = \{\mathbf{a}^{\mathcal{A}} \mid \|\mathbf{a}^{\mathcal{A}} - \bar{\mathbf{L}}_i \Theta\| = \|\mathbf{a}^{\mathcal{A}} - \bar{\mathbf{L}}_i \Theta^o\|\}$. Note that $\mathcal{A}_{\Theta, \mathbf{s}_i}$ is the vertical bisector of the segment connecting $\bar{\mathbf{L}}_i \Theta$ and $\bar{\mathbf{L}}_i \Theta^o$, which contradicts the Assumption 4. Hence, the function $\|\mathbf{d}^o(\Theta) - \mathbf{d}^o(\Theta^o)\|_t^2$ has a unique minimum at $\Theta = \Theta^o$.

Denote the objective function in (2) as $P_{M_T}(\Theta)$. We have

$$\begin{aligned} P_{M_T}(\Theta) &= \frac{1}{n} \sum_{m=1}^{M_T} \sum_{i=1}^N \frac{(d_{im}^o(\Theta^o) - d_{im}^o(\Theta) + r_{im})^2}{\sigma_{im}^2} \\ &\rightarrow \|\mathbf{d}^o(\Theta^o) - \mathbf{d}^o(\Theta)\|_t^2 + 2\langle \mathbf{d}^o(\Theta^o) - \mathbf{d}^o(\Theta), \mathbf{r} \rangle_t + \|\mathbf{r}\|_t^2 \\ &= \underbrace{\|\mathbf{d}^o(\Theta^o) - \mathbf{d}^o(\Theta)\|_t^2}_{P(\Theta)} + \|\mathbf{r}\|_t^2, \end{aligned}$$

where $\mathbf{r} \triangleq (r_j/\sigma_j)_{j=1}^\infty$, $j = (m-1)N + i$, and $\langle \mathbf{d}^o(\Theta^o) - \mathbf{d}^o(\Theta), \mathbf{r} \rangle_t = 0$ is based on [24, Theorem 3]. Note that $\hat{\Theta}_{M_T}^{\text{ML}}$ minimizes $P_{M_T}(\Theta)$ for any $M_T \in \mathbb{N}$. Then $(\hat{\Theta}_{M_T}^{\text{LS}})$ forms a sequence of minimizers of $P_{M_T}(\Theta)$. Let Θ' be a limit point of the bounded sequence $(\hat{\Theta}_{M_T}^{\text{ML}})$, and let $(\hat{\Theta}_{M_T^k}^{\text{ML}})$ be any subsequence which converges to Θ' . By the continuity of $P(\Theta)$ and the uniform convergence of $P_{M_T}(\Theta)$ to $P(\Theta) + \|\mathbf{r}\|_t^2$, $P_{M_T^k}(\hat{\Theta}_{M_T^k}^{\text{ML}}) \rightarrow P(\Theta') + \|\mathbf{r}\|_t^2$ as $k \rightarrow \infty$. Since $\hat{\Theta}_{M_T^k}^{\text{ML}}$ is the global minimizer of $P_{M_T^k}(\Theta)$, $P_{M_T^k}(\hat{\Theta}_{M_T^k}^{\text{ML}}) \leq P_{M_T^k}(\Theta^o)$. It follows that by letting $k \rightarrow \infty$, $P(\Theta') + \|\mathbf{r}\|_t^2 \leq P(\Theta^o) + \|\mathbf{r}\|_t^2 = \|\mathbf{r}\|_t^2$. Hence $P(\Theta') = 0$. As we have proved, $P(\Theta)$ has a unique minimum at Θ^o , which implies that $\Theta' = \Theta^o$. Thus for almost every \mathbf{r} , $\hat{\Theta}_{M_T}^{\text{ML}} \rightarrow \Theta^o$.

Let $l(\mathbf{d}; \Theta)$ be the log likelihood function, and denote the derivative of $l(\mathbf{d}; \Theta)$ with respect to Θ as $l'(\mathbf{d}; \Theta)$. Under the Gaussian noises Assumption 1, it holds that $l'(\mathbf{d}; \Theta^o) \xrightarrow{d} \mathcal{N}(0, \mathbf{F})$ where \mathbf{F} is the information matrix [25]. We can write the $SO(2)$ constraint as $\mathbf{f}(\Theta) = 0$ as shown in (19) and its Jacobian as $\mathbf{dF}(\Theta) \in \mathbb{R}^{3 \times 6}$. Let $\mathbf{U}(\Theta)$ be the matrix whose columns form an orthonormal null space of $\mathbf{dF}(\Theta)$, i.e., $\mathbf{dF}(\Theta)\mathbf{U}(\Theta) = 0$ and $\mathbf{U}^\top(\Theta)\mathbf{U}(\Theta) = \mathbf{I}$. Define $\mathbf{F}^*(\Theta) = \mathbf{F} + M_T \mathbf{dF}^\top(\Theta) \mathbf{dF}(\Theta)$, then given the identifiability of the problem, $\mathbf{F}^*(\Theta)$ is nonsingular [25]. Let

$$\mathbf{B}(\Theta) = \mathbf{F}^*(\Theta)^{-1}(\mathbf{F} + l''(\mathbf{d}; \Theta)),$$

$$\mathbf{Q}(\Theta) = \mathbf{F}^*(\Theta)^{-1} \mathbf{dF}(\Theta) \left(\mathbf{dF}^\top(\Theta) \mathbf{F}^*(\Theta)^{-1} \mathbf{dF}(\Theta) \right)^{-1}.$$

Since $\hat{\Theta}_{M_T}^{\text{ML}}$ is consistent, we have $\mathbf{Q}(\hat{\Theta}_{M_T}^{\text{ML}}) \xrightarrow{p} \mathbf{Q}(\Theta^o)$ and

$$\begin{aligned} \mathbf{B}(\hat{\Theta}_{M_T}^{\text{ML}}) &= \left(\frac{\mathbf{F}^*(\hat{\Theta}_{M_T}^{\text{ML}})}{M_T} \right)^{-1} \left(\frac{\mathbf{F} + l''(\mathbf{d}; \hat{\Theta}_{M_T}^{\text{ML}})}{M_T} \right) \\ &= \left(\frac{\mathbf{F}^*(\hat{\Theta}_{M_T}^{\text{ML}})}{M_T} \right)^{-1} \left(\frac{\mathbb{E}[-l''(\mathbf{d}; \Theta^o)] + l''(\mathbf{d}; \hat{\Theta}_{M_T}^{\text{ML}})}{M_T} \right) \\ &\xrightarrow{p} \mathbf{0}. \end{aligned}$$

In addition, $\mathbf{Q}(\Theta^o)$ is bounded. Then, based on [25, Theorem 3], the covariance matrix of $\hat{\Theta}_{M_T}^{\text{ML}}$ converges to $(\mathbf{I} - \mathbf{Q}(\Theta^o)\mathbf{d}\mathbf{F}^\top(\Theta^o))\mathbf{F}^*(\Theta^o)^{-1}$, which can be further transformed into [26]

$$\mathbf{U}(\Theta^o) \left(\mathbf{U}^\top(\Theta^o)\mathbf{F}\mathbf{U}(\Theta^o) \right)^{-1} \mathbf{U}^\top(\Theta^o). \quad (18)$$

Actually, (18) is the constrained Cramer-Rao lower bound (CRLB), showing the ML solution $\hat{\Theta}_{M_T}^{\text{ML}}$ that optimally solves problem (2) is asymptotically efficient. We will specifically discuss the CRLB and give the explicit expression of \mathbf{F} and $\mathbf{U}(\Theta^o)$ in Appendix F.

APPENDIX F

SO(2) CONSTRAINED CRAMER-RAO LOWER BOUND

Suppose we want to estimate the unknown vector $\Theta = (\text{vec}(\mathbf{R}), \mathbf{t}) \in \mathbb{R}^{6 \times 1}$ from the range measurements d_{im} corrupted by independent noise $r_{im} \sim \mathcal{N}(0, \sigma_{mi}^2)$ for $m = 1, 2, \dots, M_T$, and $i = 1, 2, \dots, N$, where the observations follow model (1). We can compute the CRLB for Θ as follows.

We shall first evaluate the Fisher information matrix (FIM) of the unknown parameter vector Θ without having the SO(2) constraint. The covariance matrix of any unbiased estimate of the parameter vector Θ satisfies

$$\mathbb{E}\{(\hat{\Theta} - \Theta)(\hat{\Theta} - \Theta)^\top\} \geq \mathbf{F}^{-1},$$

where \mathbf{F} is the Fisher information matrix (FIM). Let us define $\bar{\mathbf{s}}_i = [\mathbf{s}_i^\top, 1]^\top \in \mathbb{R}^3$ for $i = 1, 2, \dots, N$.

$$\mathbf{F} = \sum_{m=1}^{M_T} \sum_{i=1}^N \frac{(\bar{\mathbf{s}}_i \otimes \mathbf{I}_2)(\mathbf{a}_m - (\mathbf{R}\mathbf{s}_i + \mathbf{t}))(\mathbf{a}_m - (\mathbf{R}\mathbf{s}_i + \mathbf{t}))^\top (\bar{\mathbf{s}}_i^\top \otimes \mathbf{I}_2)}{\sigma_{mi}^2 \|\mathbf{a}_m - (\mathbf{R}\mathbf{s}_i + \mathbf{t})\|_2^2}.$$

The CRLB by imposing \mathbf{R} to SO(2) is obtained by the FIM together with the gradient matrix of the constraints with respect to Θ . Let $\mathbf{R} = [\mathbf{y}_1 \quad \mathbf{y}_2]$, the constraint $\mathbf{R} \in \text{SO}(2)$ can be expressed locally by 3 continuously differentiable constraints (with the constrained $\det(\mathbf{R}) = 1$ locally redundant):

$$\mathbf{f}(\Theta) = \begin{bmatrix} \mathbf{y}_1^\top \mathbf{y}_1 - 1 \\ \mathbf{y}_2^\top \mathbf{y}_1 \\ \mathbf{y}_2^\top \mathbf{y}_2 - 1 \end{bmatrix} = \mathbf{0}_3 \in \mathbb{R}^{3 \times 1}. \quad (19)$$

Let the gradient matrix of the constraints be defined by

$$\mathbf{d}\mathbf{f}(\theta) = \frac{\partial \mathbf{f}(\Theta)}{\partial \Theta^\top} = \begin{bmatrix} 2\mathbf{y}_1^\top & \mathbf{0}_2^\top & \mathbf{0}_2^\top \\ \mathbf{y}_2^\top & \mathbf{y}_1^\top & \mathbf{0}_2^\top \\ \mathbf{0}_2^\top & 2\mathbf{y}_2^\top & \mathbf{0}_2^\top \end{bmatrix} \in \mathbb{R}^{3 \times 6}.$$

The gradient matrix $\mathbf{d}\mathbf{f}(\theta)$ has full row rank and there exists a matrix \mathbf{U} whose columns form an orthonormal basis for the null space of $\mathbf{d}\mathbf{f}(\theta)$,

$$\mathbf{U} = \frac{1}{\sqrt{2}} \begin{bmatrix} \mathbf{y}_2 & \mathbf{O}_{4 \times 2} \\ -\mathbf{y}_1 & \\ \mathbf{0}_2 & \sqrt{2}\mathbf{I}_2 \end{bmatrix} \in \mathbb{R}^{6 \times (6-3)}$$

Given $\mathbf{U}^\top \mathbf{F} \mathbf{U}$ nonsingular, then the covariance matrix of any unbiased estimate of Θ satisfies

$$\mathbb{E}\{(\hat{\Theta} - \Theta)(\hat{\Theta} - \Theta)^\top\} \geq \mathbf{U}(\mathbf{U}^\top \mathbf{F} \mathbf{U})^{-1} \mathbf{U}^\top.$$

ACKNOWLEDGMENT

The authors would like to thank Prof Huihuan Qian, Dr. Kaiwen Xue and Mr. Jiale Zhong from The Chinese University of Hong Kong, Shenzhen, for their help in the experiment conduction.

REFERENCES

- [1] J. Zhang and S. Singh, "Low-drift and real-time lidar odometry and mapping," *Autonomous Robots*, vol. 41, no. 2, pp. 401–416, 2017.
- [2] W. Zhen and S. Scherer, "Estimating the localizability in tunnel-like environments using lidar and uwb," in *2019 International Conference on Robotics and Automation (ICRA)*. IEEE, 2019, pp. 4903–4908.
- [3] T. Shan, B. Englot, D. Meyers, W. Wang, C. Ratti, and D. Rus, "Lio-sam: Tightly-coupled lidar inertial odometry via smoothing and mapping," in *2020 IEEE/RSJ international conference on intelligent robots and systems (IROS)*. IEEE, 2020, pp. 5135–5142.
- [4] L. Schmid, D. Salido-Monzú, and A. Wieser, "Accuracy assessment and learned error mitigation of uwb tof ranging," in *2019 International Conference on Indoor Positioning and Indoor Navigation (IPIN)*. IEEE, 2019, pp. 1–8.
- [5] Y. Song, M. Guan, W. P. Tay, C. L. Law, and C. Wen, "Uwb/lidar fusion for cooperative range-only slam," in *2019 international conference on robotics and automation (ICRA)*. IEEE, 2019, pp. 6568–6574.
- [6] T.-M. Nguyen, M. Cao, S. Yuan, Y. Lyu, T. H. Nguyen, and L. Xie, "Viral-fusion: A visual-inertial-ranging-lidar sensor fusion approach," *IEEE Transactions on Robotics*, vol. 38, no. 2, pp. 958–977, 2021.
- [7] C. Wang, H. Zhang, T.-M. Nguyen, and L. Xie, "Ultra-wideband aided fast localization and mapping system," in *2017 IEEE/RSJ international conference on intelligent robots and systems (IROS)*. IEEE, 2017, pp. 1602–1609.
- [8] Y. Cao and G. Beltrame, "Vir-slam: Visual, inertial, and ranging slam for single and multi-robot systems," *Autonomous Robots*, vol. 45, no. 6, pp. 905–917, 2021.
- [9] J. González, J.-L. Blanco, C. Galindo, A. Ortiz-de Galisteo, J.-A. Fernández-Madriral, F. A. Moreno, and J. L. Martinez, "Mobile robot localization based on ultra-wide-band ranging: A particle filter approach," *Robotics and autonomous systems*, vol. 57, no. 5, pp. 496–507, 2009.
- [10] X. Fang, C. Wang, T.-M. Nguyen, and L. Xie, "Graph optimization approach to range-based localization," *IEEE Transactions on Systems, Man, and Cybernetics: Systems*, vol. 51, no. 11, pp. 6830–6841, 2020.
- [11] G. Zeng, B. Mu, J. Wei, W. S. Wong, and J. Wu, "Localizability with range-difference measurements: Numerical computation and error bound analysis," *IEEE/ACM Transactions on Networking*, 2022.
- [12] K. Xue, J. Li, N. Xiao, J. Liu, X. Ji, and H. Qian, "Improving the robot localization accuracy using range-only data: An optimization approach," in *2021 6th IEEE International Conference on Advanced Robotics and Mechatronics (ICARM)*. IEEE, 2021, pp. 785–790.
- [13] J. P. Queralta, J. Taipalmaa, B. Can Pullinen, V. K. Sarker, T. Nguyen Gia, H. Tenhunen, M. Gabbouj, J. Raitoharju, and T. West-erlund, "Collaborative multi-robot search and rescue: Planning, coordination, perception, and active vision," *IEEE Access*, vol. 8, pp. 191 617–191 643, 2020.
- [14] H.-Y. Chung, C.-C. Hou, and Y.-S. Chen, "Indoor intelligent mobile robot localization using fuzzy compensation and kalman filter to fuse the data of gyroscope and magnetometer," *IEEE Transactions on Industrial Electronics*, vol. 62, no. 10, pp. 6436–6447, 2015.
- [15] S. P. Chepuri, G. Leus, and A.-J. van der Veen, "Rigid body localization using sensor networks," *IEEE Transactions on Signal Processing*, vol. 62, no. 18, pp. 4911–4924, 2014.

- [16] S. Chen and K. Ho, "Accurate localization of a rigid body using multiple sensors and landmarks," *IEEE Transactions on Signal Processing*, vol. 63, no. 24, pp. 6459–6472, 2015.
- [17] J. Jiang, G. Wang, and K. Ho, "Sensor network-based rigid body localization via semi-definite relaxation using arrival time and doppler measurements," *IEEE Transactions on Wireless Communications*, vol. 18, no. 2, pp. 1011–1025, 2019.
- [18] B. Großwindhager, M. Stocker, M. Rath, C. A. Boano, and K. Römer, "Snaploc: An ultra-fast uwb-based indoor localization system for an unlimited number of tags," in *2019 18th ACM/IEEE International Conference on Information Processing in Sensor Networks (IPSN)*. IEEE, 2019, pp. 61–72.
- [19] J. J. Moré, "Generalizations of the trust region problem," *Optimization methods and Software*, vol. 2, no. 3-4, pp. 189–209, 1993.
- [20] G. Zeng, B. Mu, J. Chen, Z. Shi, and J. Wu, "Global and asymptotically efficient localization from range measurements," *arXiv preprint arXiv:2203.16951*, 2022.
- [21] R. Hartley, J. Trunpf, Y. Dai, and H. Li, "Rotation averaging," *International journal of computer vision*, vol. 103, no. 3, pp. 267–305, 2013.
- [22] G. Bellusci, G. J. Janssen, J. Yan, and C. C. Tiberius, "Model of distance and bandwidth dependency of toa-based uwb ranging error," in *2008 IEEE International Conference on Ultra-Wideband*, vol. 3. IEEE, 2008, pp. 193–196.
- [23] P. Billingsley, *Convergence of probability measures*. John Wiley & Sons, 2013.
- [24] R. I. Jennrich, "Asymptotic properties of non-linear least squares estimators," *The Annals of Mathematical Statistics*, vol. 40, no. 2, pp. 633–643, 1969.
- [25] M. Crowder, "On constrained maximum likelihood estimation with non-iid observations," *Annals of the Institute of Statistical Mathematics*, vol. 36, no. 1, pp. 239–249, 1984.
- [26] T. J. Moore, B. M. Sadler, and R. J. Kozick, "Maximum-likelihood estimation, the cramer-rao bound, and the method of scoring with parameter constraints," *IEEE Transactions on Signal Processing*, vol. 56, no. 3, pp. 895–908, 2008.